Deterministic global superstructure-based optimization of an organic Rankine cycle

Wolfgang R. Huster[a], Artur M. Schweidtmann[a], Jannik T. Lüthje[a], Alexander Mitsos[b,a,c,*]

[a] *Process Systems Engineering (AVT.SVT), RWTH Aachen University, 52074 Aachen, Germany*
[b] *JARA-ENERGY, Templergraben 55, 52056 Aachen, Germany*
[c] *Institute of Energy and Climate Research: Energy Systems Engineering (IEK-10), Forschungszentrum Jülich GmbH, Wilhelm-Johnen-Straße, 52425 Jülich, Germany*

Abstract

Organic Rankine cycles (ORCs) offer a high structural design flexibility. The best process structure can be identified via the optimization of a superstructure, which considers design alternatives simultaneously. In this contribution, we apply deterministic global optimization to a geothermal ORC superstructure, thus guaranteeing to find the best solution. We implement a hybrid mechanistic data-driven model, employing artificial neural networks as thermodynamic surrogate models. This approach is beneficial as we optimize the problem in a reduced space using the optimization solver MAiNGO. We further introduce redundant constraints that are only considered for the lower-bounding problem of the branch-and-bound algorithm. We perform two separate optimizations, one maximizing power output and one minimizing levelized cost of electricity. The optimal solutions of both objectives differ from each other, but both have three pressure levels. Global optimiza-

*Corresponding author: Alexander Mitsos. Tel.: +49 241 80 94704; fax: +49 241 80 92326. E-mail address: amitsos@alum.mit.edu

Preprint submitted to Journal of Computers & Chemical Engineering December 13, 2020

tion is necessary as there exist suboptimal local solutions for both flowsheet configuration and design with fixed configurations.
Keywords: Superstructure, Artificial neural network, Reduced-space formulation, Relaxation-specific constraints, MAiNGO

1. Introduction

Organic Rankine cycles (ORCs) are relevant energy processes which allow for power generation using low- to mid-temperature heat sources. They can be used for a variety of different heat sources, e.g., biomass, geothermal, or waste heat [1]. When designing ORC processes, a high number of structural process alternatives can be considered. This flexibility in the process structure allows to adjust the ORC to a heat source and ambient conditions. Although rarely applied to energy systems, superstructure optimization is a common approach in process systems engineering, which allows to include a number of discrete process variants within a single optimization problem. For ORC optimization, we consider state-equipment network formulations [2]. In general, these kind of problems can be formulated using general disjunctive programming (GDP). GDP problems can be reformulated using integer variables and yield mixed-integer nonlinear programming problems (MINLP). These problems commonly exhibit suboptimal local optima in addition to potentially multiple global optimal solutions. Local solvers cannot guarantee to find a globally optimal solution and might terminate in a suboptimal local solution. Local optima can result from the selection of integer variables, i.e., a suboptimal process structure. On the other hand, continuous optimization variables can lead to suboptimal process design for a fixed process structure.

In consequence, finding a global solution via deterministic global optimization is highly desirable for economic process design.

Reviews on MINLP and GDP formulations are given in [3, 4]. A relevant case study driving the advances in superstructure optimization is the design of heat exchanger networks (HENs) [5–8]. Starting from HENs, some groups extended the process models to the consideration of pressure changing units that produce or consume power (work and heat exchanging networks: WHENs) [9–15]. A similar approach is the use of superstructure-free approaches, in which the structural alternatives are developed during the solution procedure [16–19]. Martelli et al. [20] optimized a superstructure for finding the optimal configuration of an integrated gasification combined cycle. An overview on superstructure modeling for a variety of power generation systems is given in [21].

Furthermore, superstructure optimization has been considered for finding optimal ORC design. Schilling et al. [22] presented an approach for simultaneous optimization of working fluid and ORC process structure, and solve the resulting optimization problem using an outer-approximation strategy. Many authors decompose large-scale MINLP problems to subproblems. In [23], an outer level is solved using a genetic algorithm and a linearized inner level is solved with CPLEX. Recently, Elsido et al. [24, 25, 26, 27] presented an MINLP-MILP decomposition approach for the simultaneous optimization of ORCs and HENs, involving several heat sources. Hipólito-Valencia et al. [28, 29] presented a combination of model formulations that are solved using outer-approximation algorithms to obtain optimal designs of large-scale plants. In [30, 31], a hybrid evolutionary/traditional algorithm (HEATSEP)

is proposed. Stijepovic et al. [32] optimized ORCs based on exergy composite curves. In [33], they extended their approach to optimal working fluid selection, where they solve the linearized problem. These solution strategies can only guarantee a global solution for convex problems, which is mostly not the case, and thus, can result in a suboptimal integer solution. Deterministic global optimization has been applied for solving HENs with an integrated ORC using BARON [34, 35]. In there, the solution times are within several hours, although an ORC with a small number of structural degrees of freedom (DoF) and cubic equation of state are used.

Still, solving superstructure problems to global optimality is challenging, and there is need for appropriate formulations and solution approaches. A promising approach for deterministic global flowsheet optimization is the reduction of the number of optimization variables handled by the optimizer [36–38]. We illustrated the advantage of solving flowsheets to global optimality in a reduced-space (RS) formulation [39–41] using McCormick relaxations [42, 43]. The open-source deterministic global MINLP solver MAiNGO allows to handle models accordingly via the propagation of McCormick's relaxations, which allows to eliminate explicit model equations [44]. The optimizer handles only the actual decisions variables (and if needed, additional auxiliary optimization variables) and branches on them in the branch-and-bound (B&B) algorithm. Other model variables are hidden from the optimizer. In consequence, the size of subproblems in the lower and upping bounding problem is reduced. More detailed information is presented in [39] and [44]. Recently, Rall et al. [45] performed a superstructure optimization of a membrane process using MAiNGO, which was limited to a small number

of process variables.

A remaining challenge is the inclusion of accurate thermodynamic properties in flowsheet optimization to obtain correct optimal solution points [46]. Working in a RS, a direct implementation of complex thermodynamic models is difficult to optimize as they include implicit calculations [47–49]. We proposed using feedforward artificial neural networks (ANNs) as thermodynamic surrogate models, which can be efficiently optimized employing a RS formulation [47, 50]. For this, ANNs are trained on thermodynamic fluid data that is previously generated using thermodynamic libraries, e.g., CoolProp [51] or REFPROP [52]. The global optimization of the resulting hybrid mechanistic data-driven models showed to be viable, without introducing significant errors. We applied this method to select an optimal single-species working fluid [53] or obtain a globally optimal mixture composition [54] for ORCs.

The tightness of relaxations influences the convergence of the B&B algorithm. One option for tightening are relaxation-specific constraints [55], which are only considered in the lower-bounding problem. In here, we derive them based on physical knowledge which is implicitly enforced in the process model [56]. We further apply tailor-made relaxations for functions in process engineering that are available in MAiNGO [57]. We combine the RS formulation of a mechanistic process model of an ORC superstructure with data-driven thermodynamic models. Together with relaxation-specific constraints and tailor-made relaxations, we solve the optimization problems to global optimality. Thus, this article presents a methodology on how to solve ORC superstructure models efficiently in a reduced space. While we focus on optimal ORC design, the presented modeling strategies are not limited to

ORC systems and thus can be applied to other superstructure process models in chemical engineering. Note that the presented model formulation has been developed to be solved using the reduced-space approach in MAiNGO. To solve this superstructure with other state-of-the-art solvers such as BARON, a different model formulation would be desirable. This especially refers to the thermodynamic surrogate models, which can efficiently be solved in a reduced space [50]. Moreover, we herein utilize the parallelization of MAiNGO which other solvers do not have. We thus refrain from numerical comparisons.

The article is structured as follows. We introduce the considered superstructure in Section 2 and present the process model in Section 3, including relaxation-specific constraints, tailor-made relaxations, and the use of the ANNs. We optimize the process for a thermodynamic objective function and, subsequently, a thermoeconomic objective function and present the results in Section 4. In there, we discuss both the obtained optimal solutions as well as computational aspects. In Section 5, we summarize the approach together with the optimization results and give an outlook on future research.

2. Organic Rankine cycle superstructure

We extend the geothermal set up presented in [41, 46, 54] by integrating additional optional process units. We consider the most promising structural options for a subcritical ORC employing a single heat source that were presented in previous works [24, 27, 58]. We describe the flowsheet of the ORC superstructure (Figure 1) in the following.

The simplest ORC structure involves only necessary process units. In

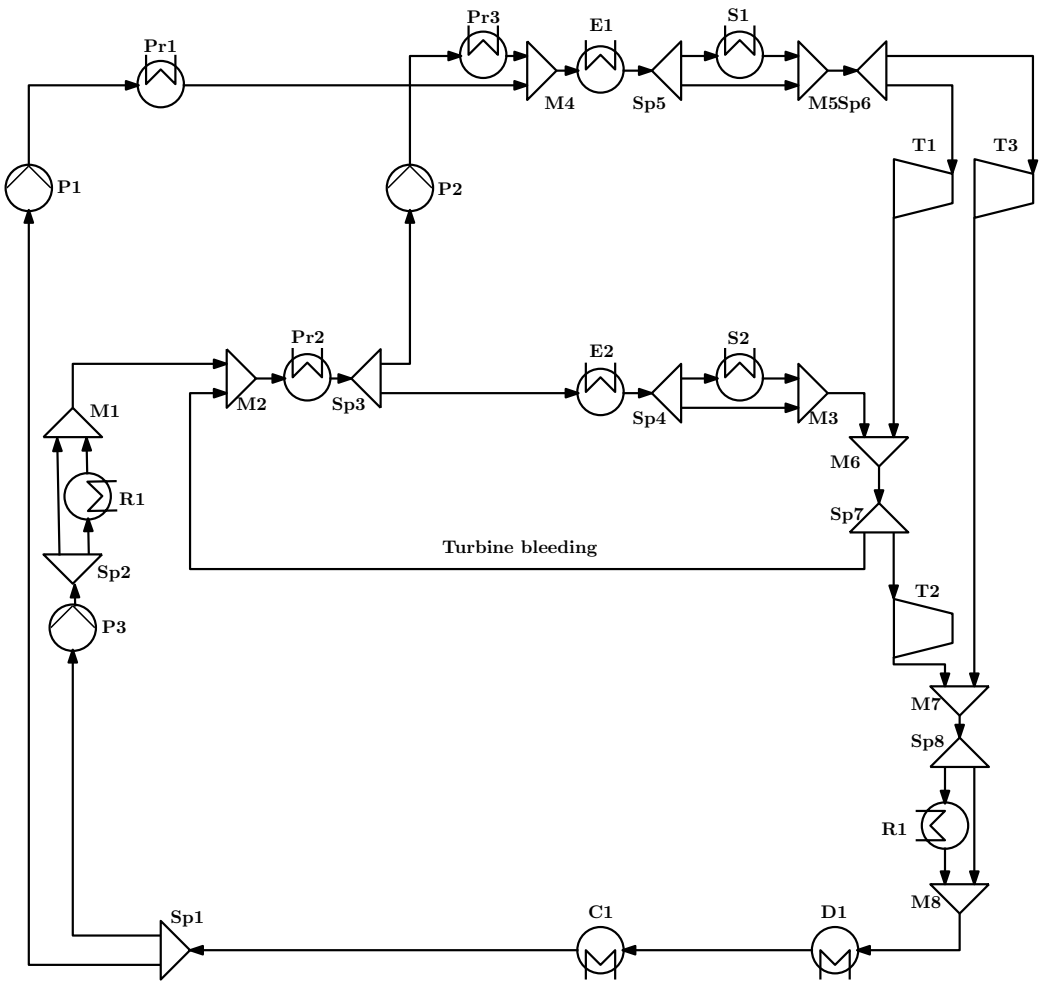

Figure 1: Flowsheet of the ORC superstructure. We use the following abbreviations: **Sp**: splitter, **P**: pump, **R**: recuperator, **M**: mixer, **Pr**: preheater, **E**: evaporator, **S**: superheater, **T**: turbine, **D**: desuperheater, **C**: condenser.

particular, the saturated liquid working fluid isobutane is pressurized from a low pressure level p_{LP} to a higher pressure level (here: medium pressure p_{MP}) using the pump **P3**. From there, the working fluid is preheated to saturated liquid temperature in the preheater **Pr2** using the geothermal brine. It is then completely evaporated (**E2**) and expanded to a lower pressure level using the turbine **T2**. The working fluid is cooled to saturation temperature (**D1**) and completely condensed (**C1**) using cooling water. We refer to this structure using the term "basic ORC".

We consider the following structural options: A recuperator **R1** can recover surplus heat after the expansion to preheat the liquid stream. Furthermore, we consider a second high pressure level p_{HP} for the working fluid (splitter **Sp1/Sp3**). If selected, a fraction of the working fluid flow is pressurized from p_{MP} to p_{HP} using pump **P2** after **Pr2**. Alternatively, it can be pressurized from p_{LP} to p_{HP} directly using pump **P1** and subsequently preheater **Pr1**. We introduce optional superheaters at p_{MP} (**S1**) and p_{HP} (**S2**). The working fluid can be expanded from p_{HP} to p_{LP} directly (**T3**). Alternatively, it can be expanded from p_{HP} to p_{MP} (**T1**) and then be mixed with the medium pressure stream (mixer **M6**). Furthermore, we consider turbine bleeding, where a stream fraction leaving **T1** is mixed with the working fluid at mixer **M2**. In this case, **E2** and **S2** are inactive.

Finally, the brine stream can be used in sequential or parallel mode. In the sequential mode, the sequence of heat exchangers for the brine stream is **S1**, **E1**, **Pr3**, **Pr1**, **S2**, **E2**, and **Pr2**. In parallel mode, the brine stream is split equally into two streams (**S1**, **E1**, **Pr3**, **Pr1** and **S2**, **E2**, **Pr2**). We do not display the brine and cooling water streams in Figure 1 for clarity.

The presented structural options correspond to a maximum number of $2^8 = 256$ potential integer combinations. However, many combinations are infeasible due to logic constraints, e.g., the nonexistence of the high pressure level discards many options. We list the logic constraints in Section 3. More structural options could be considered, e.g., a higher number of additional pressure levels. However, we select this superstructure as it encloses established structural ORC options for subcritical pressure levels making use of a single heat source.

3. Process model

In this section, we present relevant parts of the process model, i.e., the RS formulation, the incorporation of tailor-made relaxations and relaxation-specific constraints, and the thermodynamic model of the working fluid. The respective strategies are described in a way such that they can be transferred to similar process models. The process model is available in the electronic supplementary information [59]. Relevant model parameter values are summarized in Table A1. We apply standard modeling assumptions for ORC design, e.g., neglect pressure drop and heat losses. Furthermore, we assume constant heat transfer coefficients for heat exchangers and efficiencies for rotating equipment.

3.1. Reduced-space formulation of superstructure model

The selection of variables for the RS formulation of the process model can strongly influence the CPU time to solve the problem. For this, we build on insight gained in previous studies [41, 53, 54] and select as few optimization variables as possible, making use of explicit function evaluations. However,

the propagation of McCormick relaxations through complex functions can lead to weak relaxations. Thus, considering additional optimization variables can also be beneficial for the global optimization [40, 60]. The identification of an optimal formulation (hybrid formulation between full-space and RS) is ongoing research.

The basic ORC process model can be evaluated explicitly using p_{LP}, p_{MP}, and $\dot{m}_{MP}$ as DoFs. In [46], we included a superheater in the flowsheet, for which we introduced the superheat at the turbine inlet $\Delta h_{turb,in}$ as DoF. For the superstructure, we introduce one binary variable y_i in the process model for each structural option presented in Section 2. Furthermore, additional arising continuous DoFs are the high pressure level p_{HP}, the mass flow at high pressure level $\dot{m}_{HP}$, the superheat at high pressure level Δh_{S1}, and the mass-specific enthalpy at **Pr2** inlet h_{Pr2}. We select the mass flow at low pressure level $\dot{m}_{LP}$ and the mass-specific enthalpy at **T2** inlet h_{T2} as additional optimization variables to allow for explicit model evaluation. In total, the superstructure includes nine continuous and eight binary optimization variables (Table 1). In the B&B algorithm, we branch on the binary variables first, i.e., we set a branching priority of two for integer variables.

Logic constraints on binary variables are given in Table 2. In there, the first three equalities are assignments in the RS formulation, denoted by ":=". The variables on the left-hand side of the assignment are intermediate variables (as opposed to optimization variables, see [39]), i.e., they act as gray boxes to the optimizer and they are not branched on in the B&B algorithm. The displayed assignments involve bilinear integer expressions that can be reformulated to linear expressions using the Big-M method, which is com-

Table 1: Optimization variables of the reduced-space model formulation in MAiNGO. Continuous variables are listed in the upper part, binary variables in the lower part.

Variable	Unit	Bounds	Explanation
p_{LP}	bar	[2,5]	low pressure level
p_{MP}	bar	[5,22]	medium pressure level
p_{HP}	bar	[5,22]	high pressure level
$\dot{m}_{LP}$	kg/s	[5,1000]	mass flow at low pressure level
$\dot{m}_{MP}$	kg/s	[5,1000]	mass flow at medium pressure level
$\dot{m}_{HP}$	kg/s	[5,1000]	mass flow at high pressure level
Δh_{S1}	kJ/kg	[10,300]	superheat at high pressure level
h_{T2}	kJ/kg	[400,650]	enthalpy at **T2** inlet
h_{Pr2}	kJ/kg	[50,450]	enthalpy at **Pr2** inlet
y_{HP}	-	$\{0,1\}$	high pressure level
y_{Par}	-	$\{0,1\}$	brine in parallel mode
y_{TB}	-	$\{0,1\}$	turbine bleeding
y_{P2}	-	$\{0,1\}$	pump ($MP \rightarrow HP$)
y_{T3}	-	$\{0,1\}$	turbine ($HP \rightarrow LP$)
y_{R1}	-	$\{0,1\}$	recuperator
y_{S1}	-	$\{0,1\}$	superheater (HP)
y_{S2}	-	$\{0,1\}$	superheater (MP)

monly applied in GDP [61]. In our formulation, each Big-M reformulation would introduce one additional optimization variable and four inequality constraints to the optimization problem in the RS formulation. We found that the bilinear expression is computationally preferable to Big-M in our case. Relaxations of bilinear products are built in MAiNGO using McCormick's method [62, 63]. However, we use the Big-M method for the reformulation of bilinear constraints which require no additional optimization variables in the RS formulation, i.e., can be evaluated using the existing set of optimization and intermediate variables. An in-depth comparison of the methods for the RS formulation is relevant future research.

3.2. Tailor-made relaxations for selected functions in process engineering

The tightness of relaxations has a major impact on the CPU time of the B&B algorithm. In MAiNGO [44], envelopes and tight relaxations for a number of functions relevant in process engineering are available, which are stored in the MC++ library [64, 65]. We present their use within our process model in the following.

At each of the three working fluid mixing points in the superstructure (**M3**, **M7**, **M8**), we apply the `sum_div` function, which can be applied to functions of the form $(a_1 x)/(a_2 x + \sum_{i=1}^{n} b_i y_i)$ ($x, \mathbf{y}$: variables, $\mathbf{a}, \mathbf{b}$: positive parameters). The calculation of the corresponding envelopes is presented in [57]. We reformulate the energy balance around a generic mixer (Equation (1)) to obtain an explicit expression for the working fluid enthalpy at the outlet h_{out} (Equation (2)) using the `sum_div` function for both fractions

Table 2: Logic constraints for binary variables in the ORC superstructure. Note that "iff" is the abbreviation for "if and only if". We use $:=$ for assignments in the RS formulation, i.e., the intermediate variables (left-hand side) are not handled by the optimizer [39].

Equation	Explanation
$y_{P1} := y_{HP} \cdot (1 - y_{P2})$	pump **P1** is active iff high pressure level is active and pump **P2** is inactive
$y_{T1} := y_{HP} \cdot (1 - y_{T3})$	turbine **T1** is active iff high pressure level is active and turbine **T3** is inactive
$y_{Pr1} := y_{HP} \cdot (1 - y_{P2})$	preheater **Pr1** is active iff high pressure level is active and pump **P2** is inactive
$y_{Pr3} := y_{P2}$	preheater **Pr3** is active iff pump **P2** is active
$y_{E1} := y_{HP}$	evaporator **E1** is active iff high pressure level is active
$y_{Par} \leqslant y_{HP}$	parallel brine stream can only be active if high pressure level is active
$y_{S1} \leqslant y_{HP}$	superheater **S1** can only be active if high pressure level is active
$y_{T3} \leqslant y_{HP}$	turbine **T3** can only be active if high pressure level is active
$y_{TB} \leqslant y_{HP}$	turbine bleeding can only be active if high pressure level is active
$y_{TB} \leqslant y_{P2}$	turbine bleeding can only be active if pump **P2** is active
$y_{T3} + y_{TB} \leqslant 1$	turbine **T3** and turbine bleeding cannot both be active
$y_{S2} + y_{TB} \leqslant 1$	superheater **S2** and turbine bleeding cannot both be active
$y_{E2} + y_{TB} \leqslant 1$	evaporator **E2** and turbine bleeding cannot both be active
$y_{Pr2} + y_{TB} \leqslant 1$	preheater **Pr2** and turbine bleeding cannot both be active
$y_{Par} + y_{TB} \leqslant 1$	parallel brine stream and turbine bleeding cannot both be active

to provide tighter relaxations.

$$0 = (\dot{m}_{in,1} + \dot{m}_{in,2})\, h_{out} - \dot{m}_{in,1} h_{in,1} + \dot{m}_{in,2} h_{in,2} \tag{1}$$

$$\begin{aligned} h_{out} &= \frac{\dot{m}_{in,1} h_{in,1} + \dot{m}_{in,2} h_{in,2}}{\dot{m}_{in,1} + \dot{m}_{in,2}} \\ &= \frac{\dot{m}_{in,1}}{\dot{m}_{in,1} + \dot{m}_{in,2}} h_{in,1} + \frac{\dot{m}_{in,2}}{\dot{m}_{in,1} + \dot{m}_{in,2}} h_{in,2} \end{aligned} \tag{2}$$

We further use the envelopes for the mean-logarithmic temperature difference respectively its reciprocal [66, 67] for the design of each heat exchanger. Also, for the calculation of the investment costs of each process unit, we employ the envelopes for the cost function derived in [57], which are based on the cost correlations presented in [68]. In there, they reduced the CPU times for the thermoeconomic optimization of a combined-cycle power plant [39] by up to 80%. We employ a heat exchanger class, which, next to its evaluation, adds inequality constraints and relaxation-specific constraints to the overall process model. In the heat exchanger class, we eliminate redundant pinch inequality constraints if the working fluid passes two heat exchangers successionally. Finally, we use the envelopes of the hyperbolic tangent activation function used in ANNs [50].

3.3. Relaxation-specific constraints

In addition to tight function relaxations, we also apply relaxation-specific constraints that can tighten the relaxation of the overall problem [55, 56, 69, 70]. These are redundant constraints that are implicitly enforced by the pro-

cess model. Thus, they are not necessary for the solution of the problem, but they can potentially tighten the relaxations. Thus, relaxation-specific constraints are applied in the lower bounding problem and not in the upper bounding problem. They possibly can discard infeasible domains in the lower bounding problem and thus help to reduce to number of nodes the the B&B algorithm has to branch on. Implementing these redundant constraints as conventional constraints can lead to numerical difficulties for the local optimization solver. MAiNGO allows for a direct declaration of these constraints [44].

As described in the previous sections, we use binary variables to (de)activate constraints and manipulate model equations to account for different process structures. We thus expect weak relaxations for process variables whose calculation involves optional process units, as the relaxations heavily depend on the formulation of the logic constraints. In consequence, we try to tighten these relaxations using relaxation-specific constraints. For this, we include additional information based on physical insight. In our superstructure optimization problem, we implement relaxation-specific constraints which enforce mass and energy balances for different control volumes, i.e., we aggregate process units and formulate mass and energy balances for the respective model segment. The mass and energy balances around all different combinations of process units are enforced implicitly in the process model, i.e., adding them explicitly as relaxation-specific constraints can help to tighten the relaxations. We include additional reformulated energy balances around single heat exchangers, the complete ORC, the geothermal brine, single working fluid pressure levels, mixing points, and cooling water. Again, these refor-

mulations can help to tighten relaxations, as they allow to include of process knowledge which is only included implicitly in the process model. Furthermore, we use inherent knowledge based on process functionalities, e.g., introduce relaxation-specific inequality constraints that ensure increasing working fluid enthalpies along a series of heat exchanger units, which is caused by the heat transfer from the heat source. In total, we include 21 relaxation-specific equality constraints and 99 relaxation-specific inequality constraints.

3.4. Thermodynamic surrogate model of the working fluid

Accurate thermodynamic models are important for process optimization [46]. However, rigorous models often exhibit nonlinear implicit functions that lead to additional optimization variables and weak McCormick relaxations [47–49]. In our previous works [46, 47], we illustrated how feed-forward ANNs learn accurate thermodynamic properties of fluids and can be efficiently optimized as hybrid mechanistic data-driven process models in a RS formulation [50].

Thus, we use ANNs for the calculation of all working fluid properties in this work. We apply ANNs consisting of two hidden layers with four neurons for the saturated properties and two hidden layer with six neurons for the properties of subcooled liquid and superheated vapor [53]. A smaller number of neurons for the saturated properties is needed as there is less complexity in the data. We apply separate ANNs for the mentioned fluid regions with small number of neurons each, which result in tight relaxations. We omit models for the two-phase region (see [54]). They are not needed here due to isothermal phase changes of the working fluid, i.e., it is sufficient to apply pinch point inequalities for the saturated fluid states at the inlet or outlet of the

phase changing heat exchangers. In case of non-isothermal phase changes, e.g., when applying zeotropic working fluid mixtures, the pinch can occur within the heat exchanger. Enforcing the pinch inequality along the length of heat exchanger is needed in these cases, as presented in [54]. We perform the training of the ANNs in Matlab 2017b (Bayesian regularization back-propagation algorithm, 40% training, 30% validation, 30% test set). For the proposed set of ANNs, the training time is in an hourly range, thus insignificant compared to the process optimization. The artificial neural network models and illustrative training scripts are available open-source within the "MeLOn - **M**achin**e** **L**earning Models for **O**ptimizatio**n**" toolbox [71]. All ANNs and their respective accuracies on all data sets are available in the electronic supplementary information [59].

4. Results and discussion

We performed all process optimizations on an Intel(R) Core(TM) i7-4790 CPU with 3.60 GHz, 16 GB RAM, Windows 10 64 bit operating system, using MAiNGO v0.1.25 [44], with a relative optimality tolerance of 10^{-4}. The B&B algorithm terminates once the relative difference between upper and lower bound is smaller than the selected tolerance. We applied seven processes for the master-slave parallelization of the B&B algorithm. We first present the results of the thermodynamic optimization, investigate computational aspects of different solution approaches, and finally present the results of the thermoeconomic optimization.

4.1. Thermodynamic optimization

In the thermodynamic optimization, we maximize the generated net power. This selection implies that the investment costs do not influence the objective function.

4.1.1. Optimal process design

The flowsheet obtained by the thermodynamic optimization is given in Figure 2. The optimal configuration involves three pressure levels, two superheaters, and one recuperator. The results are in agreement with [41, 46], where the thermodynamic optimum suggested superheating and recuperation. Furthermore, the working fluid is pressurized from the low to the medium pressure level and from there to the high pressure level (not directly from low to high pressure level). Similarly, it is expanded from the high to the medium pressure level and from there to the low pressure level. The geothermal brine is used in the sequential mode. Thus, the active binary decision variables are y_{HP}, y_{S1}, y_{S2}, and y_{R1}. Values of relevant decision variables are given in Table 3. Table A2 in the appendix lists the states of all working fluid streams. Using this configuration, the ORC generates 19.4 MW net power. This is 17% higher compared to using no third pressure level ($P_{net,max}$ = 16.6 MW, [46]). The levelized cost of electricity $LCOE$, which are a trade-off between generated net power and investment cost [41, 53], are comparably high.

The additional pressure level can elevate the average temperature of the heat transfer, i.e., reduce exergy destruction, and thus increase the total efficiency. Figure 3 shows that the area between the geothermal brine and the working fluid in a $\dot{Q}$-T-diagram, which corresponds to exergy destruction in

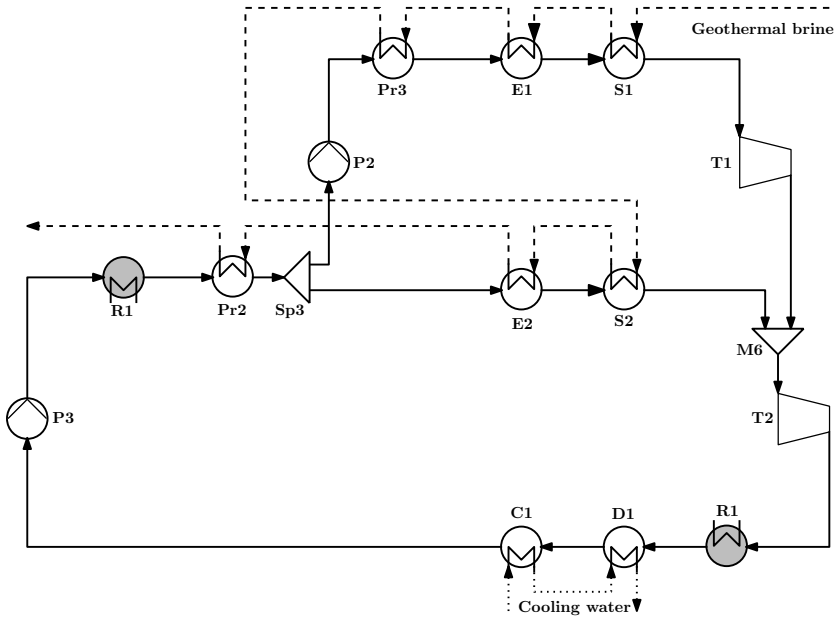

Figure 2: Optimal flowsheet of the considered ORC for $P_{net,max}$. The gray-colored heat exchangers are considered as a single process unit.

Table 3: Results of the thermodynamic optimization of the ORC.

p_{LP} [bar]	p_{MP} [bar]	p_{HP} [bar]	$\dot{m}_{MP}$ $[\frac{\text{kg}}{\text{s}}]$	$\dot{m}_{HP}$ $[\frac{\text{kg}}{\text{s}}]$	P_{T1} [MW]	P_{T2} [MW]	P_{net} [MW]	$LCOE$ $[\frac{\text{US-\$}}{\text{MWh}}]$
4.4	13.1	20.0	206.9	269.3	4.4	20.4	19.4	77.5

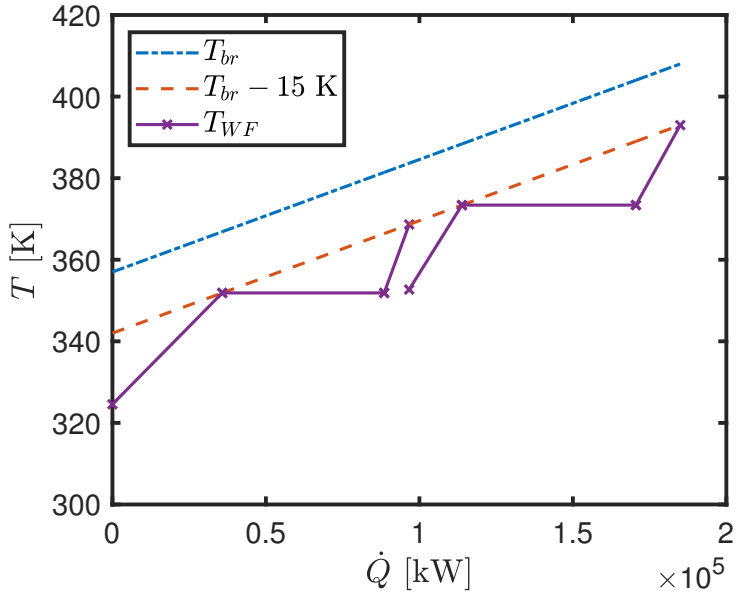

Figure 3: Resulting heat transfer from the geothermal brine to the working fluid for the thermodynamic optimization. The dashed orange line indicates the minimal temperature difference, i.e., the pinch is present at four locations.

the heat exchangers, is small. In particular, the minimum temperature difference of 15 K is present at four locations within the cycle (working fluid: MP evaporator inlet, MP superheater outlet, HP evaporator inlet, HP superheater outlet).

In the optimal process structure, expansion from high- to low-level pressure (**T3**) is not selected. The specific work that can be generated strongly depends on the specific heat capacities at different pressure levels in the superheated region. Thus, this optimal structure can hardly be determined without an optimization procedure. Also, direct pressurization from low- to high-level pressure (**P1**) and turbine bleeding are not thermodynamically preferable in this case study.

The selected ORC structure with a third pressure level, superheaters,

and a recuperator is selected in many studies in literature [1]. Although rare for small-scale plants, first ORCs with a third pressure level were realized. For large-scale Rankine cycles, e.g., combined-cycle power plants, three to four pressure levels are state-of-the-art. However, it is interesting to see that turbine bleeding and direct pressurization from low- to high-pressure level (and vice-versa) are not selected. Overall, the optimal process structure is in agreement with literature. However, the optimal structure strongly depends on many factors that are specific for each case study, such as the selection of the working fluid, and thus, the optimization provides relevant insight.

The distribution of the investment costs of the ORC units (Figure 4) illustrates that the most expensive unit is the recuperator (Inv_{R1} = m US-$ 12.0). Following to this, the turbine **T2**, the condenser **C1**, and the turbine **T1** have the highest shares (Inv_{T2} = m US-$ 7.0, Inv_{C1} = m US-$ 2.7, Inv_{T1} = m US-$ 2.3).

We applied the local MINLP solver KNITRO [72] to investigate local optima with respect to structural decisions. A single optimization that is initialized between lower and upper bound of each variable converges after 4 CPU seconds. The solution value is P_{net} = 16.7 MW, i.e., 14% less net power generation compared to the globally optimal solution. Turbine bleeding is selected in this local solution, illustrating that there exist local optima with respect to both the process structure and the design for a fixed structure. With a high number of starting points, KNITRO can identify the same solution we obtain using MAiNGO, but cannot guarantee its global optimality. While solving the problems to global optimality using MAiNGO, we observed the presence of many suboptimal local optima in all optimization set ups.

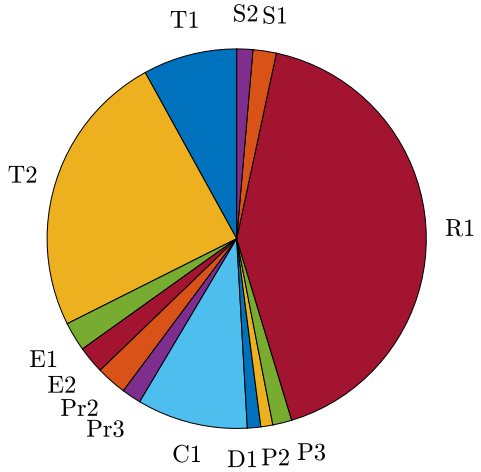

Process unit	Inv. cost [m US-$]
R1	12.03
T2	6.98
C1	2.70
T1	2.30
Pr2	0.75
E1	0.71
E2	0.67
S1	0.57
Pr3	0.47
P3	0.47
S2	0.39
D1	0.33
P2	0.29

Figure 4 & Table 4: Distribution of investment costs for $P_{net,max}$.

This highlights the need for global optimization to find both the best process structure and design.

4.1.2. Computational performance

We now compare the superstructure optimization with the brute-force approach of enumeration and global optimization of each NLP. In the NLP optimizations, we do not branch on the integer variables. Out of the 256 integer realizations, 72 are found feasible. This enumeration confirmed the optimum we obtained using the superstructure formulation.

One NLP optimization did not converge within 12 hours wall time, at which point the relative gap between lower and upper bound was at 3.6%. However, the lower bound was inferior to the global solution of the MINLP when the optimization was terminated. Thus, in Table 5, we sum over the converged solutions of feasible structures and add the time of the manually

terminated optimization. We neglect infeasible combinations as the time for proving infeasibility is less than 3 seconds. Furthermore, we give the computational properties of the superstructure optimization with and without relaxation-specific constraints (Table 5). The use of relaxation-specific constraints reduces the number of B&B iterations by 39% compared to not using them, which is a result of tighter relaxations of the feasible region. The CPU time for solving the MINLP problem is reduced by 49%. For the enumeration of the flowsheets, we also included the presented relaxation-specific constraints. These results illustrate the potential of solving superstructure formulations with relaxation-specific constraints embedded.

Table 5: Computational results of the thermodynamic optimization of the ORC using different modeling approaches. The CPU time is the sum over all cores in the parallelized B&B algorithm.

Approach	B&B iterations	CPU time in hours
Enumeration	$4.1 \cdot 10^7$	485
Superstructure w/o rel.-spec. constr.	$1.8 \cdot 10^7$	590
Superstructure with rel.-spec. constr.	$1.1 \cdot 10^7$	292

4.2. Thermoeconomic optimization

In the thermoeconomic optimization, we minimize $LCOE$. This objective function can account for a trade-off between the thermodynamic optimal design and investment cost, as shown in [53].

The results of the thermoeconomic optimization suggest a similar optimal ORC structure as the thermodynamic optimization (Figure 5). The major differences are the nonexistence of the recuperator and both superheaters. The results for the ORC structure are in agreement with the observations

made in [41]. Note that we investigated only two pressure levels in [41]. In consequence, the high number of structural options in here can basically result in a different combination of superheaters and/or recuperator.

While P_{net} is only reduced by 5% compared to the thermodynamic optimization, the ORC investment cost can be reduced from m US-$ 28.6 to m US-$ 15.2. The $LCOE$ are reduced from 77.5 US-$/MWh ($P_{net,max}$) to 61.2 US-$/MWh ($LCOE_{min}$). By selecting the additional pressure level, $LCOE$ can be reduced by 4% compared to the basic ORC ($LCOE_{min,basic}$ = 63.8 US-$/MWh).

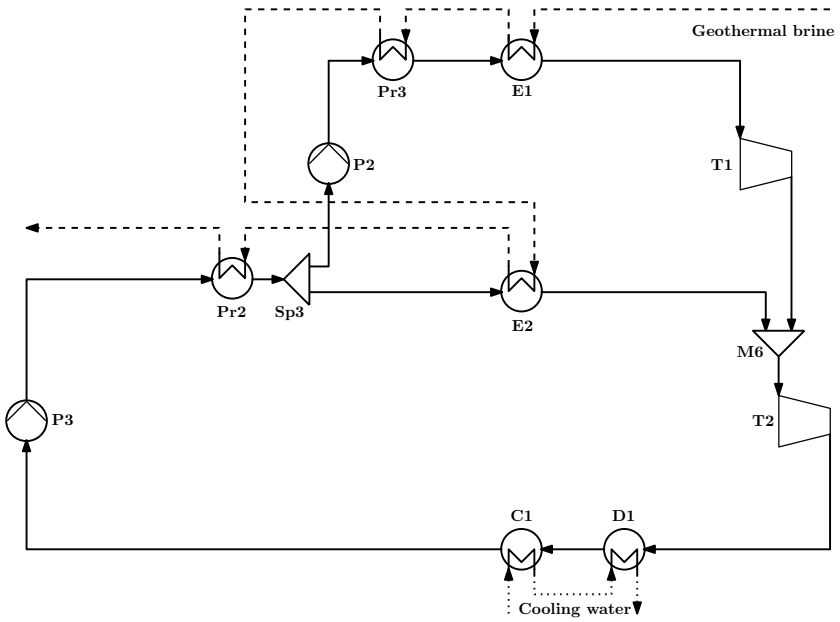

Figure 5: Optimal flowsheet of the considered ORC for $LCOE_{min}$.

All three pressure levels and mass flows are close to the thermodynamic optimum (Table 6). All working fluid states are listed in Table A2 in the appendix. Figure 6 illustrates that more exergy is destroyed in the heat transfer between working fluid and brine, as the areas between the curves are larger

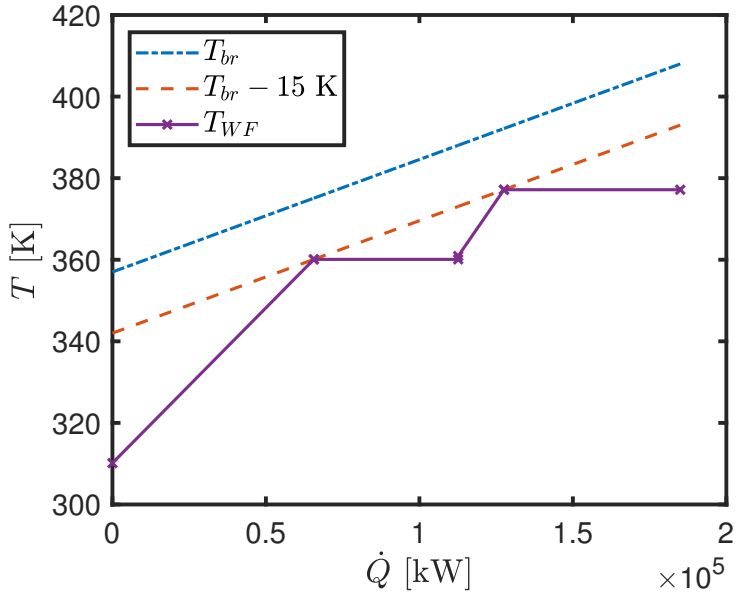

Figure 6: Resulting heat transfer from the geothermal brine to the working fluid for the thermoeconomic optimization. The dashed orange line indicates the minimal temperature difference, i.e., the pinch is present at two locations.

than in Figure 3. The minimum temperature difference is only present at two locations (working fluid: MP evaporator inlet, HP evaporator inlet).

Table 6: Results of the thermoeconomic optimization of the ORC.

p_{LP} [bar]	p_{MP} [bar]	p_{HP} [bar]	$\dot{m}_{MP}$ [$\frac{\text{kg}}{\text{s}}$]	$\dot{m}_{HP}$ [$\frac{\text{kg}}{\text{s}}$]	P_{T1} [MW]	P_{T2} [MW]	P_{net} [MW]	$LCOE$ [$\frac{\text{US-\$}}{\text{MWh}}$]
4.8	15.5	21.4	196.3	285.8	3.0	20.1	18.5	61.2

The turbine **T2**, the condenser **C1**, and the turbine **T1** have the highest share of investment costs (Inv_{T2} = m US-$ 6.9, Inv_{C1} = m US-$ 2.5, Inv_{T1} = m US-$ 1.8) (Figure 7).

The thermoeconomic optimization converged within 783 CPU hours ($1.9 \cdot 10^7$ B&B iterations, 115 hours wall clock time). As in similar problems [41,

53, 54], the thermoeconomic optimization needs more CPU time than the thermodynamic optimization, which is mostly due to a more complicated objective function. We only investigated the results of the superstructure optimization with relaxation-specific constraints, as this showed to be the fastest approach for solving the flowsheet optimization (see Section 4.1.2).

A local optimization with KNITRO converges after 39 CPU seconds. It results in an objective value of $LCOE = 64.6$ US-$/MWh, for which a different ORC structure is selected, e.g., **T3** is active instead of **T2**. KNITRO can identify the same solution as MAiNGO with an increased number of starting points.

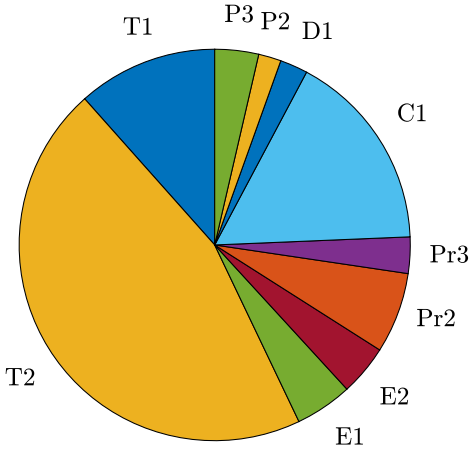

Process unit	Inv. cost [m US-$]
T2	6.92
C1	2.52
T1	1.76
Pr2	1.01
E1	0.72
E2	0.63
P3	0.55
Pr3	0.46
D1	0.35
P2	0.28

Figure 7 & Table 7: Distribution of investment cost for $LCOE_{min}$.

5. Conclusion

We present a strategy for solving complex nonlinear superstructure problems to guaranteed global optimality. In particular, we consider four modeling aspects that significantly influence the solution time. First, we formu-

late the superstructure model in a reduced-space which reduces the number of variables and constraints handled by the optimizer. Second, we employ tailor-made relaxations for selected functions in process engineering. Third, we implement relaxation-specific constraints based on process insight that tighten the relaxations of the feasible region. Fourth, we apply ANNs as accurate thermodynamic models which can be efficiently solved in the reduced-space formulation. In addition, we use the parallelization of our open-source solver MAiNGO.

The described solution strategies can be applied for solving superstructure process models in chemical and energy engineering. In here, we demonstrate the approach for an ORC superstructure that includes 2^8 possible structural integer combinations. Using the proposed strategy, we solve the thermodynamic and thermoeconomic process optimization within 44 and 115 hours wall-clock time, respectively. Particularly, we find that the relaxation-specific constraints reduce CPU times by up to 49%.

The optimal ORC configuration generates 17% more net power than a basic ORC configuration. Using a thermoeconomic objective function, we can reduce investment costs by 47% compared to the thermodynamic optimum, while the generated net power is only reduced by 5%. Although differing process structures are selected, selecting three pressure levels is beneficial for both objective functions, as it allows to reduce the exergy destruction of the heat transfer. The obtained process structures are selected in many studies in literature, but not yet state-of-the-art in most plants, which could be due to additional control measures. Several suboptimal local optima were observed, which justifies the need for solving ORC design problems with deterministic

global optimization solvers.

Authors' contribution. AM initiated the idea of solving superstructure ORC models using deterministic global optimization. WRH, AMS and JTL developed the approach. WRH and JTL implemented the model within MAiNGO. WRH and AMS wrote the manuscript, JTL and AM edited.

Acknowledgments. The authors gratefully acknowledge the financial support of the Kopernikus project SynErgie by the Federal Ministry of Education and Research (BMBF) and the project supervision by the project management organization Projektträger Jülich (PtJ). Simulations were performed with computing resources granted by RWTH Aachen University under project thes0611. The authors would like to thank Dominik Bongartz for the discussions and proofreading.

References

[1] E. Macchi, M. Astolfi (Eds.), Organic Rankine cycle (ORC) power systems, Elsevier, 2017.

[2] H. Yeomans, I. E. Grossmann, A systematic modeling framework of superstructure optimization in process synthesis, Computers & Chemical Engineering 23 (1999) 709–731.

[3] F. Trespalacios, I. Grossmann, Review of mixed-integer nonlinear and generalized disjunctive programming methods, Chemie Ingenieur Technik 86 (2014) 991–1012.

[4] Q. Chen, I. Grossmann, Recent developments and challenges in optimization-based process synthesis, Annual Review of Chemical and Biomolecular Engineering 8 (2017) 249–283.

[5] T. Yee, I. Grossmann, Z. Kravanja, Simultaneous optimization models for heat integration-I. Area and energy targeting and modeling of multi-stream exchangers, Computers & Chemical Engineering 14 (1990) 1151–1164.

[6] T. Yee, I. Grossmann, Simultaneous optimization models for heat integration-II. Heat exchanger network synthesis, Computers & Chemical Engineering 14 (1990) 1165–1184.

[7] T. Yee, I. Grossmann, Z. Kravanja, Simultaneous optimization models for heat integration-III. Process and heat exchanger network optimization, Computers & Chemical Engineering 14 (1990) 1185–1200.

[8] K. C. Furman, N. V. Sahinidis, A critical review and annotated bibliography for heat exchanger network synthesis in the 20th century, Industrial & Engineering Chemistry Research 41 (2002) 2335–2370.

[9] H. Yu, J. Eason, L. T. Biegler, X. Feng, Simultaneous heat integration and techno-economic optimization of organic Rankine cycle (ORC) for multiple waste heat stream recovery, Energy 119 (2017) 322–333.

[10] H. Yu, C. Fu, M. Vikse, C. He, T. Gundersen, Identifying optimal thermodynamic paths in work and heat exchange network synthesis, AIChE Journal 65 (2018) 549–561.

[11] H. Yu, M. Vikse, T. Gundersen, Comparison of reformulations of the Duran-Grossmann model for work and heat exchange network (WHEN) synthesis, in: Computer Aided Chemical Engineering, Elsevier, 2018, pp. 489–494.

[12] H. Yu, C. Fu, M. Vikse, T. Gundersen, Work and heat integration—a new field in process synthesis and process systems engineering, AIChE Journal 65 (2018) e16477.

[13] J. Li, S. E. Demirel, M. M. F. Hasan, Process integration using block superstructure, Industrial & Engineering Chemistry Research 57 (2018) 4377–4398.

[14] J. Li, S. E. Demirel, M. M. F. Hasan, Process synthesis using block superstructure with automated flowsheet generation and optimization, AIChE Journal 64 (2018) 3082–3100.

[15] J. Li, S. E. Demirel, M. M. F. Hasan, Building block-based synthesis and intensification of work-heat exchanger networks (WHENS), Processes 7 (2019) 23.

[16] P. Voll, M. Lampe, G. Wrobel, A. Bardow, Superstructure-free synthesis and optimization of distributed industrial energy supply systems, Energy 45 (2012) 424–435.

[17] P. Voll, C. Klaffke, M. Hennen, A. Bardow, Automated superstructure-based synthesis and optimization of distributed energy supply systems, Energy 50 (2013) 374–388.

[18] L. Wang, P. Voll, M. Lampe, Y. Yang, A. Bardow, Superstructure-free synthesis and optimization of thermal power plants, Energy 91 (2015) 700–711.

[19] L. Wang, M. Lampe, P. Voll, Y. Yang, A. Bardow, Multi-objective

superstructure-free synthesis and optimization of thermal power plants, Energy 116 (2016) 1104–1116.

[20] E. Martelli, C. Elsido, A. Mian, F. Marechal, MINLP model and two-stage algorithm for the simultaneous synthesis of heat exchanger networks, utility systems and heat recovery cycles, Computers & Chemical Engineering 106 (2017) 663–689.

[21] C. Frangopoulos, M. Von Spakovsky, E. Sciubba, A brief review of methods for the design and synthesis optimization of energy systems, International Journal of Thermodynamics 5 (2002) 151–160.

[22] J. Schilling, C. Horend, A. Bardow, Integrating superstructure-based design of molecules, processes and flowsheets, AIChE Journal (2019), in press.

[23] M. Kermani, A. S. Wallerand, I. D. Kantor, F. Maréchal, Generic superstructure synthesis of organic Rankine cycles for waste heat recovery in industrial processes, Applied Energy 212 (2018) 1203–1225.

[24] C. Elsido, A. Mian, E. Martelli, A systematic methodology for the techno-economic optimization of organic Rankine cycles, Energy Procedia 129 (2017) 26–33.

[25] C. Elsido, A. Bischi, P. Silva, E. Martelli, Two-stage MINLP algorithm for the optimal synthesis and design of networks of CHP units, Energy 121 (2017) 403–426.

[26] C. Elsido, E. Martelli, I. E. Grossmann, A bilevel decomposition method for the simultaneous synthesis of utility systems, Rankine cycles and

heat exchanger networks, in: Computer Aided Chemical Engineering, Elsevier, 2018, pp. 373–378.

[27] C. Elsido, E. Martelli, I. E. Grossmann, A bilevel decomposition method for the simultaneous heat integration and synthesis of steam/organic Rankine cycles, Computers & Chemical Engineering 128 (2019) 228–245.

[28] B. J. Hipólito-Valencia, E. Rubio-Castro, J. M. Ponce-Ortega, M. Serna-González, F. Nápoles-Rivera, M. M. El-Halwagi, Optimal integration of organic Rankine cycles with industrial processes, Energy Conversion and Management 73 (2013) 285–302.

[29] B. J. Hipólito-Valencia, E. Rubio-Castro, J. M. Ponce-Ortega, M. Serna-González, F. Nápoles-Rivera, M. M. El-Halwagi, Optimal design of inter-plant waste energy integration, Applied Thermal Engineering 62 (2014) 633–652.

[30] A. Toffolo, A synthesis/design optimization algorithm for Rankine cycle based energy systems, Energy 66 (2014) 115–127.

[31] A. Lazzaretto, G. Manente, A. Toffolo, SYNTHSEP: A general methodology for the synthesis of energy system configurations beyond superstructures, Energy 147 (2018) 924–949.

[32] M. Z. Stijepovic, A. I. Papadopoulos, P. Linke, A. S. Grujic, P. Seferlis, An exergy composite curves approach for the design of optimum multi-pressure organic Rankine cycle processes, Energy 69 (2014) 285–298.

[33] M. Z. Stijepovic, A. I. Papadopoulos, P. Linke, V. Stijepovic, A. S. Grujic, M. Kijevčanin, P. Seferlis, Organic Rankine cycle system performance targeting and design for multiple heat sources with simultaneous working fluid selection, Journal of Cleaner Production 142 (2017) 1950–1970.

[34] C.-L. Chen, F.-Y. Chang, T.-H. Chao, H.-C. Chen, J.-Y. Lee, Heat-exchanger network synthesis involving organic Rankine cycle for waste heat recovery, Industrial & Engineering Chemistry Research 53 (2014) 16924–16936.

[35] C.-L. Chen, P.-Y. Li, S. N. T. Le, Organic Rankine cycle for waste heat recovery in a refinery, Industrial & Engineering Chemistry Research 55 (2016) 3262–3275.

[36] S. Balendra, I. D. L. Bogle, Modular global optimisation in chemical engineering, Journal of Global Optimization 45 (2009) 169–185.

[37] R. Byrne, I. Bogle, Global optimization of modular process flowsheets, Industrial & Engineering Chemistry Research 39 (2000) 4296–4301.

[38] T. G. W. Epperly, E. N. Pistikopoulos, A reduced space branch and bound algorithm for global optimization, Journal of Global Optimization 11 (1997) 287–311.

[39] D. Bongartz, A. Mitsos, Deterministic global optimization of process flowsheets in a reduced space using McCormick relaxations, Journal of Global Optimization 20 (2017) 419.

[40] D. Bongartz, A. Mitsos, Infeasible path global flowsheet optimization using McCormick relaxations, in: A. Espuna (Ed.), 27th European Symposium on Computer Aided Process Engineering, volume 40 of *Computer Aided Chemical Engineering*, Elsevier, San Diego, 2017.

[41] W. R. Huster, D. Bongartz, A. Mitsos, Deterministic global optimization of the design of a geothermal organic Rankine cycle, Energy Procedia 129 (2017) 50–57.

[42] G. P. McCormick, Computability of global solutions to factorable nonconvex programs: Part I – Convex underestimating problems, Mathematical Programming 10 (1976) 147–175.

[43] A. Mitsos, B. Chachuat, P. I. Barton, McCormick-based relaxations of algorithms, SIAM Journal on Optimization 20 (2009) 573–601.

[44] D. Bongartz, J. Najman, S. Sass, A. Mitsos, MAiNGO – McCormick-based Algorithm for mixed-integer Nonlinear Global Optimization, Technical Report, Process Systems Engineering (AVT.SVT), RWTH Aachen University, 2018, `http://permalink.avt.rwth-aachen.de/?id=729717`.

[45] D. Rall, A. M. Schweidtmann, M. Kruse, E. Evdochenko, A. Mitsos, M. Wessling, Multi-scale membrane process optimization with high-fidelity ion transport models through machine learning, Journal of Membrane Science (2020) 118208.

[46] W. R. Huster, A. M. Schweidtmann, A. Mitsos, Impact of accurate working fluid properties on the globally optimal design of an organic

Rankine cycle, in: Computer Aided Chemical Engineering, Elsevier, 2019, pp. 427–432.

[47] A. M. Schweidtmann, W. R. Huster, J. T. Lüthje, A. Mitsos, Deterministic global process optimization: Accurate (single-species) properties via artificial neural networks, Computers & Chemical Engineering 121 (2018) 67–74.

[48] A. M. Schweidtmann, D. Bongartz, W. R. Huster, A. Mitsos, Deterministic global process optimization: Flash calculations via artificial neural networks, in: Computer Aided Chemical Engineering, volume 46, Elsevier, 2019, pp. 937–942.

[49] D. Bongartz, A. Mitsos, Deterministic global flowsheet optimization: Between equation-oriented and sequential-modular methods, AIChE Journal 65 (2019) 1022–1034.

[50] A. M. Schweidtmann, A. Mitsos, Deterministic global optimization with artificial neural networks embedded, Journal of Optimization Theory and Applications 180 (2019) 925–948.

[51] I. H. Bell, J. Wronski, S. Quoilin, V. Lemort, Pure and pseudo-pure fluid thermophysical property evaluation and the open-source thermophysical property library CoolProp, Industrial & Engineering Chemistry Research 53 (2014) 2498–2508.

[52] E. W. Lemmon, I. H. Bell, M. L. Huber, M. O. McLinden, NIST Standard Reference Database 23: Reference Fluid Thermodynamic and

Transport Properties-REFPROP, Version 10.0, National Institute of Standards and Technology, 2018.

[53] W. R. Huster, A. M. Schweidtmann, A. Mitsos, Working fluid selection for organic Rankine cycles via deterministic global optimization of design and operation, Optimization and Engineering 21 (2020) 517–536.

[54] W. R. Huster, A. M. Schweidtmann, A. Mitsos, Globally optimal working fluid mixture composition for geothermal power cycles (2020), , submitted September 6th, 2019.

[55] N. V. Sahinidis, M. Tawarmalani, Accelerating branch-and-bound through a modeling language construct for relaxation-specific constraints, Journal of Global Optimization 32 (2005) 259–280.

[56] J. P. Ruiz, I. E. Grossmann, Using redundancy to strengthen the relaxation for the global optimization of MINLP problems, Computers & Chemical Engineering 35 (2011) 2729–2740.

[57] J. Najman, D. Bongartz, A. Mitsos, Relaxations of thermodynamic property and costing models in process engineering, Computers & Chemical Engineering 130 (2019) 106571.

[58] S. Lecompte, H. Huisseune, M. van den Broek, B. Vanslambrouck, M. D. Paepe, Review of organic Rankine cycle (ORC) architectures for waste heat recovery, Renewable and Sustainable Energy Reviews 47 (2015) 448–461.

[59] W. R. Huster, A. M. Schweidtmann, A. Mitsos, Electronic supplementary information of "Deterministic global superstructure-based opti-

mization of an organic Rankine cycle", 2020. URL: http://permalink.avt.rwth-aachen.de/?id=843237.

[60] D. T. Doncevic, A. M. Schweidtmann, Y. Vaupel, P. Schäfer, A. Caspari, A. Mitsos, Deterministic global nonlinear model predictive control with neural networks embedded, Submitted to IFAC (2020).

[61] I. E. Grossmann, F. Trespalacios, Systematic modeling of discrete-continuous optimization models through generalized disjunctive programming, AIChE Journal 59 (2013) 3276–3295.

[62] A. Tsoukalas, A. Mitsos, Multivariate McCormick relaxations, Journal of Global Optimization 59 (2014) 633–662.

[63] J. Najman, A. Mitsos, Convergence analysis of multivariate McCormick-relaxations, Journal of Global Optimization 66 (2016) 597–628.

[64] B. Chachuat, MC++ (version 2.0): A toolkit for bounding factorable functions, 2014. URL: http://omega-icl.bitbucket.org/mcpp/.

[65] B. Chachuat, B. Houska, R. Paulen, N. Peri'c, J. Rajyaguru, M. E. Villanueva, Set-theoretic approaches in analysis, estimation and control of nonlinear systems, IFAC-PapersOnLine 48 (2015) 981–995.

[66] J. Najman, A. Mitsos, Convergence order of McCormick relaxations of LMTD function in heat exchanger networks, in: Z. Kravanja (Ed.), 26th European Symposium on Computer Aided Process Engineering, volume 38 of *Computer Aided Chemical Engineering*, Elsevier, Amsterdam, Netherlands, 2016, pp. 1605–1610.

[67] M. Mistry, R. Misener, Optimising heat exchanger network synthesis using convexity properties of the logarithmic mean temperature difference, Computers & Chemical Engineering 94 (2016) 1–17.

[68] R. Turton, R. C. Bailie, W. B. Whiting, J. A. Shaeiwitz, D. Bhattacharyya, Analysis, Synthesis and Design of Chemical Processes (4th Edition) (Prentice Hall International Series in the Physical and Chemical Engineering Sciences), Prentice Hall, 2012.

[69] J. P. Ruiz, I. E. Grossmann, Exploiting vector space properties to strengthen the relaxation of bilinear programs arising in the global optimization of process networks, Optimization Letters 5 (2010) 1–11.

[70] E. Ahmetović, I. E. Grossmann, Global superstructure optimization for the design of integrated process water networks, AIChE Journal 57 (2011) 434–457.

[71] A. M. Schweidtmann, L. Netze, A. Mitsos, MeLOn: Machine Learning Models for Optimization, `https://git.rwth-aachen.de/avt.svt/public/MeLOn/`, 2020.

[72] R. H. Byrd, J. Nocedal, R. A. Waltz, Knitro: An integrated package for nonlinear optimization, in: Nonconvex Optimization and Its Applications, Springer US, 2006, pp. 35–59.

[73] M. Lukawski, Design and optimization of standardized organic Rankine cycle power plant for european conditions, MA thesis, RES- The School for Renewable Energy Science, 2010.

Appendix A. Tables

Table A1: Model assumptions for the geothermal case study. Please note that assumptions on heat exchanger properties are selected based on the contacting fluid regimes. We select their values in accordance with [41] to ensure comparability.

Parameter	Unit	Value
$T_{br,in}$	K	408
$T_{br,out}$	K	357
$(\dot{m} \cdot c_p)_{br}$	kW/K	3627
$T_{cw,in}$	K	288
$\Delta T_{p,evap,pre,SH}$	K	15
$\Delta T_{p,cond,dSH}$	K	10
$\Delta T_{p,recup}$	K	10
α_{preh}	kW/(m^2 K)	1.1
α_{evap}	kW/(m^2 K)	2
α_{SH}	kW/(m^2 K)	0.7
α_{cond}	kW/(m^2 K)	1.6
α_{dSH}	kW/(m^2 K)	1.6
α_{recup}	kW/(m^2 K)	0.06
$\eta_{is,T}$	-	0.9
$\eta_{mech,T}$	-	0.8
$\eta_{is,pump}$	-	0.9

Appendix B. Economic model

In the following, we present the economic model, which is based on [41]. We minimize levelized cost of electricity in the thermoeconomic optimization:

$$LCOE = \frac{Inv_{total} \cdot \Psi \cdot \varphi}{P_{net} \cdot T_{eq}} + u_{var}, \tag{B.1}$$

with the sum of the investment cost Inv_{total}. We assume the other factors to be constant: the equivalent utilization time at rated power $T_{eq} = 8000$ h/a, an annuity factor $\Psi = 0.2$ 1/a, a fixed operation cost factor $\varphi = 1.06$ and a variable cost factor $u_{var} = 4$ US-$/MWh.

Table A2: Working fluid conditions for the globally optimal solutions of the thermodynamic ($P_{net,max}$) and thermoeconomic ($LCOE_{min}$) optimization.

Process unit	Location	$P_{net,max}$			$LCOE_{min}$		
		p [bar]	T [K]	$\dot{m}$ [kg/s]	p [bar]	T [K]	$\dot{m}$ [kg/s]
P3	inlet	4.4	307	476.2	4.8	309	482.1
P3	outlet	13.1	307	476.2	15.5	310	482.1
Pr2	inlet	13.1	325	476.2	15.5	408	482.1
Pr2	outlet	13.1	352	476.2	15.5	360	482.1
P2	inlet	13.1	352	269.3	15.5	360	285.8
P2	outlet	20.0	353	269.3	21.4	361	285.8
Pr3	outlet	20.0	373	269.3	21.4	377	285.8
E1	outlet	20.0	373	269.3	21.4	377	285.8
S1	outlet	20.0	393	269.3	-	-	-
T1	outlet	13.1	377	269.3	15.5	362	285.8
E2	inlet	13.1	352	206.9	15.5	360	196.3
E2	outlet	13.1	352	206.9	15.5	360	196.3
S2	outlet	13.1	369	206.9	-	-	-
M6	outlet	13.1	373	476.2	15.5	361	482.1
T2	outlet	4.4	340	476.2	4.8	321	482.1
D1	inlet	4.4	317	476.2	4.8	321	482.1
D1	outlet	4.4	307	476.2	4.8	309	482.1

We determine the heat exchanger area and its respective base purchase cost $C_{p,i}$ based on the mean logarithmic temperature difference and the heat transfer rate. The investment cost of a heat exchanger $Inv_{hx,i}$ is calculated in combination with a pressure factor $F_{p,i}$ [68]:

$$Inv_{hx,i} = 1.18 \cdot (1.63 + 1.66 \cdot 2.75 \cdot F_{p,i}) \cdot C_{p,i}. \tag{B.2}$$

For the investment cost of the pumps Inv_{pump}, the turbines Inv_{turb}, and a cooling tower Inv_{tower}, which is included to account for heat-sink related

cost, based on the consumed/produced power [73]:

$$\frac{Inv_{pump}}{\mathrm{US}-\$} = 3540 \cdot \left(\frac{P_{pump}}{\mathrm{kW}}\right)^{0.71} \tag{B.3}$$

$$\frac{Inv_{turb}}{\mathrm{US}-\$} = 6000 \cdot \left(\frac{P_{turb}}{\mathrm{kW}}\right)^{0.7} + 60 \cdot \left(\frac{P_{turb}}{\mathrm{kW}}\right)^{0.95} \tag{B.4}$$

$$\frac{Inv_{tower}}{\mathrm{US}-\$} = 1.5 \cdot 10^5 \cdot \left(\frac{P_{fan}}{P_{fan,0}}\right)^{0.6} \tag{B.5}$$